Biophysical Journal, Volume 98

Supporting Material

Independent and cooperative motions of the Kv1.2 channel: Voltage-sensing and gating

Adva Yeheskel, Turkan Haliloglu, and Nir Ben-Tal

SUPPORTING MATERIAL

The PDs of different K-channels are similar, but VSDs may be different

Several x-ray structures of Kv channels are available. Jiang et al determined the structure of the KvAP channel in its open conformation (1). The protein was crystallized with monoclonal antibodies. The S3-S4 paddles are located near the intracellular membrane surface, perpendicular to the pore axis. Lee et al. also determined the structure of KvAP in its open conformation (2). In this structure the S3-S4 loop was determined to be outside the membrane, because it was crystallized in a micelle. The protein was crystallized with Fv fragments but the conformation was similar to the crystals without Fv fragments in a lower resolution (2). Lee et al created a model structure of KvAP based on the two previous KvAP structures (1, 2) as it would be in a lipid bilayer (2). Long et al determined the structure of the Kv1.2 channel in its open/inactivated state (3). On one hand, the location of the C-terminus of S6 helix is in the open state. On the other hand, two of the S4 arginines are buried in the protein whereas the other two are exposed to the lipid. This state of S4 helix refers to the inactive conformation. Some of the amino acid positions in the loops between the helices of the VSD are missing. Furthermore, the positions of specific residues in S2 and S3 are missing.

Yarov-Yarovoy et al. built a model structure of the Kv1.2 channel (4), based on the X-ray crystal structure of reference (1) using the ROSETTA software package. We used their model structure here. They also modeled the closed state using the experimental evidence that E226 in S2 is positioned near R294 in the S4 helix in the closed state (5). The group also modeled the open state of KvAP using the x-ray structure (1) and the closed state of Kv1.2 as a template.

Laine et al. created a model structure of the open state of *Shaker* (6), using the PD from the x-ray structure of MthK, which was determined in its open state (7). The model for interaction between the domains was developed using molecular dynamics simulated annealing procedure. In this model the charged S4 helix was predicted to be located between the PDs from different subunits rather than in the periphery of the protein. Loops between the helices of the sensor domain were not included in this model structure and the helices of the sensor domain were all straight.

Pathak et al created a new ROSETTA model structure of Kv1.2 (8) which is similar to the former model (4), but with different loops. The model was based on the results of fluorescence scan.

Long et al determined the structure of a chimera protein composed of rat Kv1.2 with the S3b-S4 paddle from the rat Kv2.1 (9).

A comparison of these structures has shown that the PD is similar in all structures and the differences are mainly in the sensor domain.

Dependence of the fluctuation modes on the structure

The majority of the calculations were conducted using the model structure of Kv1.2 in its open state. Nevertheless, the hinges were observed also in other structures of the channel. Various x-ray structures and model structures of voltage gated potassium channels were published (2, 4, 6, 8-10). In all the structures analyzed here the three slowest modes display similar contribution to the overall dynamics of the open model of Kv1.2.

In the three slowest modes of the last KvAP structure ((2), PDB 2a0l) no hinge between the S3 and S4 helices was detected. In the next five modes a hinge near L129 (in the middle of the S4 helix) appeared, in addition to a hinge between the S3a and S3b helices (P99). This implies that the S3b and S4 helices form a rigid element, as in Kv1.2. The hinge in P99 is consistent with the Biotin-Avidin experiments (11). The three slowest modes represent the opening of the pore with hinges in the selectivity filter, M217-G222 (the S6 helix) and T160-F184 (the S5 helix). In these modes, hinges in the end of the S1 helix (T47) and between the S3a and S3b helices (G101) were also detected. Overall, the hinges are consistent with these observed in the Kv1.2 model structure. Other modeled structures of KvAP (2, 4) showed the same motions. Papazian's KvAP model (6) showed different motions. In the three slowest modes of this model structure there are hinges in the S2 helix (F279), the S4 helix (M356), the S5 helix (G406), the selectivity filter (W434-D447) and the S6 helix (L468-T469). The hinges in the S5 and S6 helices are located in the interface between these helices, similar to the hinges in Kv1.2. The hinge in the S4 helix appears in its C-terminus rather than between the arginines as in Kv1.2. Loops between the helices of the sensor are not included in this model and the four

helices of the VSD are all straight. Therefore, we cannot expect to have motions similar to the other model structures.

The fluctuations of Yarov-Yarovoy's closed model structure of Kv1.2 (4) were identical to the three slowest modes of the open model structure, which was analyzed here. The exception is that the C-terminus of the S6 helix was less mobile in the closed model, which may be expected with the increase in the contacts between the termini of the helices in the closed state. Reassuringly, the mean square fluctuations of the closed model are also similar to those of the open model (Figure S10).

In the three slowest modes of Pathak's Kv1.2 model structure (8) the hinge in the S2 helix (S217) was missing. The fluctuations of the rest of the protein were identical to Yarov-Yarovoy's Kv1.2 model. This model differs from Yarov-Yarovoy's model only in the loops between the helices of the VSD.

In the three slowest modes of the Kv7.1 model structure (10), which was based on Yarov-Yarovoy's Kv1.2 as a template, hinges of the PD were identical to the hinges in Kv1.2. The hinges in the VSD were different: a hinge between the S1 and S2 helices appeared in the three slowest modes (Q147). In the next mode this hinge disappeared and two hinges in the S1 and S2 helices appeared (L137-S140 and T153 respectively). The hinge in the S3 helix appeared in the middle of the helix (I204), next to the hinge in the S4 helix (I235), which appeared between the arginine residues. Still, the two helices moved as a rigid unit.

In the three slowest modes of the chimera structure of Kv1.2 and Kv2.1 (9), there was another hinge in the loop between helices S1 and S2. This structure differs from Yarov-Yarovoy's Kv1.2 model in the loops between the helices of the VSD.

Elastic Network Models

We analyzed the Kv1.2 model structure using the Gaussian Network Model (GNM) (12, 13) and Anisotropic Network Model (ANM) (14, 15). GNM is known as more robust in the mean-square fluctuations (16). Thus, it was used here to predict the relative magnitudes of fluctuations of the amino acids to identify hinge regions. The correlation between the fluctuations in the slowest modes of motion was used to predict the cooperation between the rigid structural elements. The eight slowest modes, further

decomposed into the first three and the next five, were chosen for the analysis based on the distribution of the eigenvalues (Fig. S2).

ANM was then used to predict the directions of motions and to generate the conformations that describe the fluctuations in 3D in the corresponding modes. The mean-square fluctuations by GNM and ANM were compared to find the corresponding modes (15, 17). The calculations were conducted with distance cutoffs of 10 and 15Å for the GNM and ANM calculations, respectively. The HingeProt webserver ((15); http://www.prc.boun.edu.tr/appserv/prc/HingeProt3/index.html) was utilized in the calculations together with in house GNM/ANM programs.

GNM

The protein structure is simplified into alpha-carbon atoms and is treated as a three-dimensional elastic network. The residues within a cutoff distance are connected by Hookean springs with a uniform force constant γ. Residues i and j are assumed to display Gaussian fluctuations about their mean positions in the separation $\mathbf{R}_{ij} = |\mathbf{R}_j - \mathbf{R}_i|$, where $\mathbf{R}_i$ and $\mathbf{R}_j$ are the respective position vectors of the ith and jth C_α-atoms.

The correlation between the fluctuations of residues i and j, $\Delta\mathbf{R}_i$ and $\Delta\mathbf{R}_j$ is calculated (12, 13) as follows

$$< \Delta\mathbf{R}_i \, \Delta\mathbf{R}_j > = (3k_B T/\gamma) \, [\mathbf{\Gamma}^{-1}]_{ij} = (3k_B T/\gamma) \, \Sigma_k \, [\lambda_k^{-1} \, \mathbf{u}_k \, \mathbf{u}^T{}_k \,]_{ij} \qquad (1)$$

Here $\mathbf{\Gamma}$ is the connectivity matrix (or Kirchhoff) matrix. λ_k is the k–th eigenvalue of $\mathbf{\Gamma}$ and is representative of the frequency of the k-th mode of motion. $\mathbf{u}_k$ is k-th eigenvector, k_B is the Boltzmann constant and T is the absolute temperature in degrees Kelvin. This equation provides a way to decompose the dynamics into N-1 eigenmodes for N interacting residues. The contribution of each motion is scaled with the inverse frequency of that mode. The slowest modes thus contribute most to the predicted fluctuations. A few slowest modes were shown to be collective and possibly relevant to the functionality of the biomolecules (17).

The global and local minima points in the fluctuations profiles of each mode are referred to hinge points. The structural segments which are connected by hinge points form rigid parts.

The dynamic correlations are calculated by the cross-correlations between the fluctuations of each pair of amino acids (12, 13). The correlation between $\Delta\mathbf{R}_i$ and $\Delta\mathbf{R}_j$ is calculated using equation 1, with $i \neq j$. This analysis is used to identify cooperative motions between different segments within the monomer and between the monomers.

Specific pairs of amino acids, in the interfaces between the monomers, were excluded from the calculation to identify the region which affects the cooperation in motion.

ANM

Here $\mathbf{\Gamma}$ is replaced by Hessian matrix $\mathbf{H}$ of the second derivative of the intramolecular potential function in eq 1. $\mathbf{H}$ is 3N×3N symmetric matrix. The correlation between $\Delta\mathbf{R}_i$ and $\Delta\mathbf{R}_j$ decomposed into 3N-6 modes of motions is then calculated as follows

$$< \Delta\mathbf{R}_i . \Delta\mathbf{R}_j> = (3k_BT/\gamma)\ tr\ [\mathbf{H}^{-1}] = (3k_BT/\gamma)\ \Sigma_k\ tr[\lambda_k^{-1}\ \mathbf{u}_k\ \mathbf{u}^T_k\ ]_{ij} \quad (2)$$

$tr[\mathbf{H}^{-1}]_{ij}$ is the trace of the ij^{th} submatrix $[\mathbf{H}^{-1}]_{ij}$ of $\mathbf{H}^{-1}$. It refers to the three different components of $\Delta\mathbf{R}_i$ and $\Delta\mathbf{R}_j$; whereas, when i=j, the self correlations between the components $\Delta\mathbf{R}_i$ are obtained. Here the fluctuation vectors allows to construct and explicitly view pairs of alternative conformations sampled by the individual modes, simply by adding the fluctuation vectors $\pm\Delta\mathbf{R}_i$ to the equilibrium position vectors in the respective modes.

Limitations of the method

In both GNM and ANM, a protein structure, simplified into C-alpha atoms, is treated as an elastic network of residues connected by hookean springs within a cutoff distance. The model has two main underlying simplifications; the absence of the

specificity in the inter-residue interactions and the inadequacy for describing the nonlinear motions. The contribution of the specificity of a residue to the motion could be only through its impact on the structure's topology.

Evolutionary conservation

The degree of evolutionary conservation of each residue was calculated using the ConSeq web-server ((18); http://conseq.tau.ac.il/). We used rat Kv1.2 as the input sequence. A multiple sequence alignment of homologous proteins was built by MUSCLE (19) using 125 homologous sequences from the SWISSPROT database (20). The alignment, available in http://ibis.tau.ac.il/wiki/nir_bental/index.php/Adva, contains the nine Kv channels sub-families as well as calcium activated K-channels and other voltage gated cation channels. The conservation scores of the amino acid positions were estimated using an empirical Bayesian inference method (21). The results were color-coded on the sequence using the key in Fig. S1. The multiple sequence alignment was also used to identify polymorphism between Kv channels within positions which are located close to hinge points.

Residues near the PD hinges which were found to be important

The three slowest modes suggested two hinges in the PD, near the two gates of the channel: The first (residues I402-V410) is near the internal gate of the S6 helix, and the second (T373-D379) is in the selectivity filter. These hinges allow the opening of the pore. Several residues in these regions were found to be conserved and involved in various syndromes, as elaborated here.

P382, located near the selectivity filter, is highly conserved (Fig. S1). A mutation of the equivalent position in human Kv7.1, a homologous channel that is expressed mainly in the heart and ear, from proline to alanine is associated with long QT syndrome type 1 (LQT1) (22). The side chain of this amino acid points toward G387 (of S6 helix) which is also conserved as glycine.

Adjacent to this hinge region, M372 is also conserved (although a bit less than P382 and G387). This position, which accommodates also leucine or valine, is in close

proximity to G338 of the S5 helix and G398 of the S6 helix. A mutation of the corresponding position in Kv7.1 (V310I) also causes LQT1 (22).

Near the selectivity filer, S371 is highly conserved. The only other amino acid in this position in potassium channels is threonine, which is very similar to serine. Na^+ channels contain hydrophobic amino acids in this position (See the MSA in http://ibis.tau.ac.il/wiki/nir_bental/index.php/Adva). S371 is in close proximity to Y377 of the near neighbor monomer. Y377 is part of the GYG motif of the selectivity filter and is highly conserved. The corresponding position in human Kv7.1 is a threonine. Substitution to arginine causes LQT1 in human (22). This mutation may perturb the hydrogen-bond between S/T371 and Y377.

Residues near the hinge between the domains which were found to be important

The hinge appears between the S4-S5 linker and the S5 helix, around residues M325-L328 (Fig. 1; marked as 4). The sequence analysis identified two conserved residues, E327 and L328, in this region (Fig. S1). E327 of rat Kv1.2 corresponds to E261 in the paralogous Kv7.1 in human. The E261D and E261K mutants of Kv7.1 are associated with Jervell and Lange-Nielsen syndrome (JLNS) and Long QT syndrome type 1 (LQT1), respectively (22, 23). Adjacent to this hinge region, S324 is also conserved (Fig. S1). This position, which accommodates only serine, histidine or cysteine, is in the S5 helix, in close proximity to V408 and I409 in the S6 helix. The later positions are also conserved (Fig. S1) and the three residues appear to interact via hydrogen-bonds.

Hinges in the VSD

The three hinges in the VSD suggested by the first three GNM modes are around C181 of the S1 helix, S217 of the S2 helix and V261 of the S3 helix (Fig. 1). In the next five modes these hinges shift toward the middle of their respective helices (data not shown). Moreover, in these modes, the same hinges appear to be effective in cooperative motion. Thus, one may envision motion of the helices around the S4 helix. The hinge in the S3 helix is consistent with structural and Biotin-Avidin binding data in the KvAP homologue. The data suggested that the S3 helix is made of two regions: S3a and S3b,

and that the S3a helix remains static whereas the S3b and S4 helices move together when the channel gates (11, 24). The ANM results in the corresponding modes revealed that the S1 and S2 helices move as a rigid unit, in a similar way to the S3-S4 paddle (Movie S1)

The VSD is autonomous

The calculations for the isolated VSD demonstrate the modularity of the Kv channels. Approximately, the hinges that were found to govern the motion of the VSD in the whole channel were also found in the isolated VSD. The hinges were found in the vicinity of residues I177 (helix S1), F180 (helix S1), E226 (helix S2), Y266 (helix S3) and R300 (helix S4). The motion of the isolated VSD might thus be sufficient to translate voltage changes into gate closing.

ANM analysis of the isolated VSD revealed several interesting modes of motions. In one mode the identified hinges are located in the middle of the helices. The outer part of the VSD, near the extracellular region, moves clockwise (extracellular view), whereas the inner part, near the intracellular region, moves counterclockwise. This motion reminds the iris-like motion of the whole Kv1.2 tetramer. In another mode the loops between helices S1-S2 and S3-S4 move in different directions. This motion is similar to an opening of a funnel - the extracellular mouth of the VSD opens wider. Both types of motions may help to visualize how the VSD acts as a proton channel. Nevertheless, these motions might be limited in the whole channel due to the contacts between the VSDs and the PDs.

Comparison between normal mode analysis and the Pathrover method

The Pathrover algorithm generates low-energy paths between two conformations using an all-atom representation of the protein structures (25, 26). Both normal mode analysis and Pathrover are fast and allow exploring the motions of a protein with a solved structure. Both relay on a known protein structure. Normal mode analysis using GNM and ANM give the fluctuations around the conformation and may give hints about more relevant conformations. In contrast, Pathrover requires a second conformation, or at least partial

structural information about a second conformation. When used, Pathrover would extract the most plausable way to get to the second conformation.

TABLES

Table S1: The rigid elements as identified by the first three GNM modes

Residues	Location in 2a79
A162-C181	The N-terminus of the S1 helix
L182-S217	Loop S1-S2
F218-V261	The S2 helix and the S2-S3 loop
A262-S324	The S3, S4 helices and the S4-S5 linker
G329-M372	The S5 helix and part of the pore loop
M380-T401	The pore loop and the N-terminus of the S6 helix
S411-T421	The C-terminus of the S6 helix

The rigid elements are connected by the hinges which are presented in Table S2.

Table S2: The hinges as identified by first three GNM modes

Hinge index	Residues	Location in 2a79
1	C181	The S1 helix
2	S217	The S2 helix
3	V261	The S3 helix
4	M325-L328	The S5 helix
5	T373-D379	The selectivity filter
6	I402-V410	The S6 helix

Table S3: The hinges as identified by GNM modes 4-8

Hinge index	Residues	Location in 2a79
1	L174-V178	The S1 helix
2	V225	The S2 helix
3	P265	The S3 helix
4	F302	The S4 helix
5	G338-F348	The S5 helix
6	F365	The pore helix
7	T373-N379	The selectivity filter
8	G386-A395	The S6 helix
9	E420	The S6 helix

Table S4: Matching GNM and ANM modes

Hinge index	Third GNM mode	First ANM mode	Fifth ANM mode	Fourth GNM mode	Fifth GNM mode	Fourth ANM mode
1	C181	C181	L182	V178	V172-L174	F180
2	S217	C229	T216	F223	W232-S234	T227
3	V261	I254	I254-T269	P265	I264-P265	T269
4	M325-L328	R326	L321	V301	F302-R303	R300
5	T373-D379	T374-V375	T373-G376	L341-F348	S343-V346	A345
6	I402-V410	I402	A403	V390	V381-I389	V390

The hinges in the slowest GNM modes and the corresponding ANM modes, identified by the mean-square fluctuations' profiles. It is evident that the third GNM mode (which is also similar to the average over modes 1, 2 and 3) corresponds to the first and fifth ANM modes. The second and third ANM modes are degenerate and together show the same motion as the first ANM mode. The fourth ANM mode corresponds to the fourth and fifth GNM mode.

Table S5: Evolutionarily correlated positions

KvAP	rKv1.2	Location in 2a79
I18	M171	Helix S1
D20	I173	Helix S1
L103	T264	Helix S3
H109	A275	Loop S3-S4
A111	K277	Loop S3-S4
V240	H418	Helix S6
E242	E420	Helix S6

Evolutionary correlated positions in KvAP (27), the homologous positions in rat Kv1.2 and the locations of these positions in the rat Kv1.2 structure (PDB 2a79).

FIGURE LEGENDS

Figure S1

ConSeq analysis of rat Kv1.2. The sequence is colored using the conservation scale at the bottom: variable residues are in turquoise, conserved residues are in burgundy. The two arrows near the N- and C- termini mark the boundaries of the structure, and the locations

of the S1-to-S6 helices are indicated. The S4 arginines and selectivity filter are marked by asterisks. Important hinge points and regions of restricted mobility are marked by colored rectangles: 302 in orange (the S4 helix), 325-328 in dark blue (the S5 helix), 373-379 in green (the pore loop) and 402-410 in blue (the S6 helix). The transmembrane segments S1-through-S6 are conserved and show a helical conservation pattern, as anticipated. The loops between the helices of the VSD (S1-S4) are variable. Most of the hinge regions are conserved.

Figure S2

The contribution of the first 50 GNM fluctuation modes to the overall motion of the tetramer. The percentage of contribution was estimated as the weight of the frequency of a specific mode, calculated considering the frequencies of all modes ($100\lambda_1 / \lambda_{n-1}$). The first three modes have the highest contribution to the overall motion. Their fraction contributions add up to 14.6%. The next five modes (4-8) contribute 7.68% to the overall motion.

Figure S3

Comparison of the dynamic correlations and mean square fluctuations of all 1040 modes vs. the average of the eight slowest modes. (a) Intramolecular and intermolecular cross-correlations of the tetramer (average over modes 1-1040). The locations of the four monomers are marked on the axes. (b) Intramolecular and intermolecular cross-correlations of the tetramer (average over modes 1-8). (c) Intramolecular cross-correlations over modes 1-1040. (d) Intramolecular cross-correlations over modes 1-8. The locations of the two domains are marked on the axes. The magnitude of the positive and negative correlations between the fluctuations of the amino acids is color-coded using the red-through-blue scale on the right of each panel. (e) Mean-square fluctuations of the Kv1.2 model-structure in the eight slowest modes (black) and in all modes (gray). The helix locations are marked on the x-axis. Analysis of all modes of motion did not add more information beyond the slowest eight modes.

Figure S4

The model structure of a Kv1.2 monomer colored by the cross-correlations between the fluctuations of residues in the C-terminus of the S6 helix and the rest of the monomer, in modes 4-8 (see Fig. 3 *d*). The color key is the same as in Fig. 3. The motions of the internal gate and the selectivity filter are positively correlated. The figure was prepared using Pymol (28).

Figure S5

Comparison of the correlated fluctuations of an isolated VSD to these of a VSD within the context of the tetramer. (a) Intramolecular cross-correlations of the isolated VSD (average over modes 1-2). (b) Intramolecular cross-correlations of the voltage sensor within the context of the full tetramer (average over modes 4-12). The locations of the S1-S4 helices are marked. The color key is the same as in Fig. 3. The correlations within the VSD are very similar, indicating the independent motion of this domain even within the context of the whole channel.

Figure S6

Comparison of the correlated fluctuations of an isolated monomer to these of the monomer within the context of the tetramer. (a) Intramolecular cross-correlations of the tetramer (average over modes 1-10). (b) Intramolecular cross-correlations of the isolated monomer (average over modes 1-3). The correlation between the S6 and S4 helices are marked by the brown rectangles. The correlations of the selectivity filter with the rest of the protein are marked by the white rectangles. The color key is the same as in Fig. 3. The locations of the domains are marked on the axes. The positive correlation between the selectivity filter and the VSD, observed within the tetramer, disappears in the monomer. The negative correlation between the S6 and S4 helices is higher in the monomer.

Figure S7

A comparison of intra molecular correlated fluctuations in the whole tetramer to these of the tetramer in the absence of contacts between S4 and S5 of the neighbor monomer. (a)

Intramolecular cross-correlations of the whole tetramer (average over modes 4-8). (b) Intramolecular cross-correlations of the tetramer in the absence of contacts between S4 and S5 of the neighbor monomer (average over modes 4-8). Positive and negative correlations between the fluctuations of the amino acids are colored red and blue, respectively. The locations of the domains are marked on the axes. The correlations between residues of the VSD in each monomer are the same even in the absence of contacts between S4 and S5 of the neighbor monomer. However, the loss of this interface affects the correlations between the VSD and PD and inside the PD. The voltage sensing motion is unaffected but the coupling between the two domains and the coupling inside the PD are different

Figure S8

The 3D structure of a monomeric Kv1.2 colored by the cross-correlations between the fluctuations of residues in the N-terminus of the S1 helix and the rest of the monomer, in modes 4-8 (see Figure 3 *d*). The colors key is the same as in Fig. 3. Residues of the S1 helix are positively correlated with other functional regions, including the S4 helix and the internal gate in helix S6. The picture was prepared using Pymol (28).

Figure S9

Comparison of the correlated fluctuations of an isolated monomer to these of the monomer within the context of the tetramer. (a) Intramolecular cross-correlations of the tetramer (average over modes 1-10). (b) Intramolecular cross-correlations of the isolated monomer (average over modes 1-3). The positive and negative correlations between the fluctuations of the amino acids are marked in red and blue. The locations of the domains are marked on the axes. The positive correlation between the selectivity filter and the VSD, observed within the tetramer, disappears in the monomer. This correlation is marked by a black rectangle.

Figure S10

Comparison between the mean square fluctuations of the open Kv1.2 model-structure (black) and the closed Kv1.2 model-structure (red). (a) Mean-square fluctuations in the three slowest modes. (b) Mean square fluctuations in modes 4-8.

Movie S1

Two movies of the motion, obtained using ANM, are available online at:
http://ibis.tau.ac.il/wiki/nir_bental/index.php/Adva
The motion toward the opening of the pore was inferred by the forth ANM mode. The ANM fluctuations display motion of the cytoplasmic region (*red*) of the protein in a clockwise direction (from the extracellular side), whereas the other region (*blue*) moves counterclockwise. The hinges are located in positions F180, T227, T269, R300, A345, V390. (a) A top view from the extracellular side. (b) A side view. The motion in this mode shows the opening and closing of the pore together with the motion of the paddle. The movies were generated using Pymol (28).

REFERENCES

1. Jiang, Y., A. Lee, J. Chen, V. Ruta, M. Cadene et al. 2003. X-ray structure of a voltage-dependent K+ channel. Nature 423:33-41.
2. Lee, S. Y., A. Lee, J. Chen, and R. MacKinnon. 2005. Structure of the KvAP voltage-dependent K+ channel and its dependence on the lipid membrane. Proceedings of the National Academy of Sciences of the United States of America 102:15441-15446.
3. Long, S. B., E. B. Campbell, and R. Mackinnon. 2005. Crystal structure of a mammalian voltage-dependent Shaker family K+ channel. Science (New York, N.Y 309:897-903.
4. Yarov-Yarovoy, V., D. Baker, and W. A. Catterall. 2006. Voltage sensor conformations in the open and closed states in ROSETTA structural models of K(+) channels. Proceedings of the National Academy of Sciences of the United States of America 103:7292-7297.
5. Tombola, F., M. M. Pathak, and E. Y. Isacoff. 2005. Voltage-sensing arginines in a potassium channel permeate and occlude cation-selective pores. Neuron 45:379-388.
6. Laine, M., M. C. Lin, J. P. Bannister, W. R. Silverman, A. F. Mock et al. 2003. Atomic proximity between S4 segment and pore domain in Shaker potassium channels. Neuron 39:467-481.

7. Jiang, Y., A. Lee, J. Chen, M. Cadene, B. T. Chait et al. 2002. Crystal structure and mechanism of a calcium-gated potassium channel. Nature 417:515-522.
8. Pathak, M. M., V. Yarov-Yarovoy, G. Agarwal, B. Roux, P. Barth et al. 2007. Closing in on the resting state of the Shaker K(+) channel. Neuron 56:124-140.
9. Long, S. B., X. Tao, E. B. Campbell, and R. MacKinnon. 2007. Atomic structure of a voltage-dependent K+ channel in a lipid membrane-like environment. Nature 450:376-382.
10. Smith, J. A., C. G. Vanoye, A. L. George, Jr., J. Meiler, and C. R. Sanders. 2007. Structural models for the KCNQ1 voltage-gated potassium channel. Biochemistry 46:14141-14152.
11. Banerjee, A., and R. MacKinnon. 2008. Inferred motions of the S3a helix during voltage-dependent K+ channel gating. Journal of molecular biology 381:569-580.
12. Bahar, I., A. R. Atilgan, and B. Erman. 1997. Direct evaluation of thermal fluctuations in proteins using a single-parameter harmonic potential. Folding & design 2:173-181.
13. Haliloglu, T., Bahar I and Erman B. 1997. Gaussian dynamics of folded proteins. Physical review letters 79:3090-3093.
14. Atilgan, A. R., S. R. Durell, R. L. Jernigan, M. C. Demirel, O. Keskin et al. 2001. Anisotropy of fluctuation dynamics of proteins with an elastic network model. Biophysical journal 80:505-515.
15. Emekli, U., D. Schneidman-Duhovny, H. J. Wolfson, R. Nussinov, and T. Haliloglu. 2008. HingeProt: automated prediction of hinges in protein structures. Proteins 70:1219-1227.
16. Cui, Q., and I. Bahar. 2006. Normal Mode Analysis: Theory and Applications to Biological and Chemical Systems. Boca Raton : Chapman & Hall/CRC.
17. Bahar, I., and A. J. Rader. 2005. Coarse-grained normal mode analysis in structural biology. Current opinion in structural biology 15:586-592.
18. Berezin, C., F. Glaser, J. Rosenberg, I. Paz, T. Pupko et al. 2004. ConSeq: the identification of functionally and structurally important residues in protein sequences. Bioinformatics (Oxford, England) 20:1322-1324.
19. Edgar, R. C. 2004. MUSCLE: multiple sequence alignment with high accuracy and high throughput. Nucleic acids research 32:1792-1797.
20. Bairoch, A., B. Boeckmann, S. Ferro, and E. Gasteiger. 2004. Swiss-Prot: juggling between evolution and stability. Briefings in bioinformatics 5:39-55.
21. Mayrose, I., D. Graur, N. Ben-Tal, and T. Pupko. 2004. Comparison of site-specific rate-inference methods for protein sequences: empirical Bayesian methods are superior. Molecular biology and evolution 21:1781-1791.
22. Tranebjaerg, L., J. Bathen, J. Tyson, and M. Bitner-Glindzicz. 1999. Jervell and Lange-Nielsen syndrome: a Norwegian perspective. American journal of medical genetics 89:137-146.
23. Franqueza, L., M. Lin, J. Shen, I. Splawski, M. T. Keating et al. 1999. Long QT syndrome-associated mutations in the S4-S5 linker of KvLQT1 potassium channels modify gating and interaction with minK subunits. The journal of biological chemistry 274:21063-21070.

24. Ruta, V., J. Chen, and R. MacKinnon. 2005. Calibrated measurement of gating-charge arginine displacement in the KvAP voltage-dependent K+ channel. Cell 123:463-475.
25. Enosh, A., B. Raveh, O. Furman-Schueler, D. Halperin, and N. Ben-Tal. 2008. Generation, comparison, and merging of pathways between protein conformations: gating in K-channels. Biophysical journal 95:3850-3860.
26. Raveh, B., A. Enosh, O. Schueler-Furman, and D. Halperin. 2009. Rapid sampling of molecular motions with prior information constraints. PLoS Comput Biol 5:e1000295.
27. Fleishman, S. J., O. Yifrach, and N. Ben-Tal. 2004. An evolutionarily conserved network of amino acids mediates gating in voltage-dependent potassium channels. Journal of molecular biology 340:307-318.
28. DeLano, W. L. 2002. PyMol Molecular Graphics System. DeLano Scientific, Palo Alto, CA, USA.

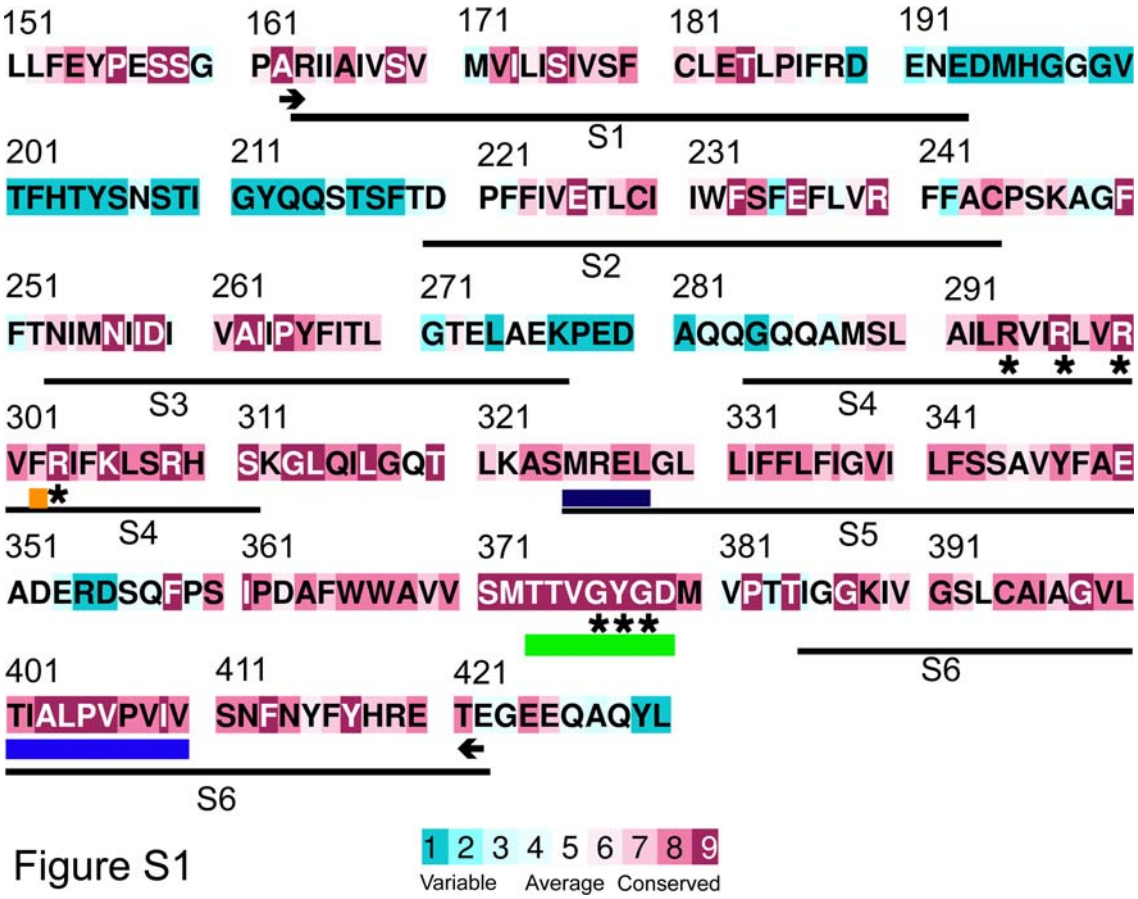
151
161
171
181
191
LLFEYPESSG
PARIIAIVSV
MVILISIVSF
CLETLPIFRD
ENEDMHGGGV
S1
201
211
221
231
241
TFHTYSNSTI
GYQQSTSFTD
PFFIVETLCI
IWFSFEFLVR
FFACPSKAGF
S2
251
261
271
281
291
FTNIMNIDI
VAIPYFITL
GTELAEKPED
AQQGQQAMSL
AILRVIRLVR
S3
S4
301
311
321
331
341
VFRIFKLSRH
SKGLQILGQT
LKASMRELGL
LIFFLFIGVI
LFSSAVYFAE
S4
S5
351
361
371
381
391
ADERDSQFPS
IPDAFWWAVV
SMTTVGYGDM
VPTTIGGKIV
GSLCAIAGVL
S6
401
411
421
TIALPVPVIV
SNFNYFYHRE
TEGEEQAQYL
S6
1 2 3 4 5 6 7 8 9
Variable
Average
Conserved

Figure S1

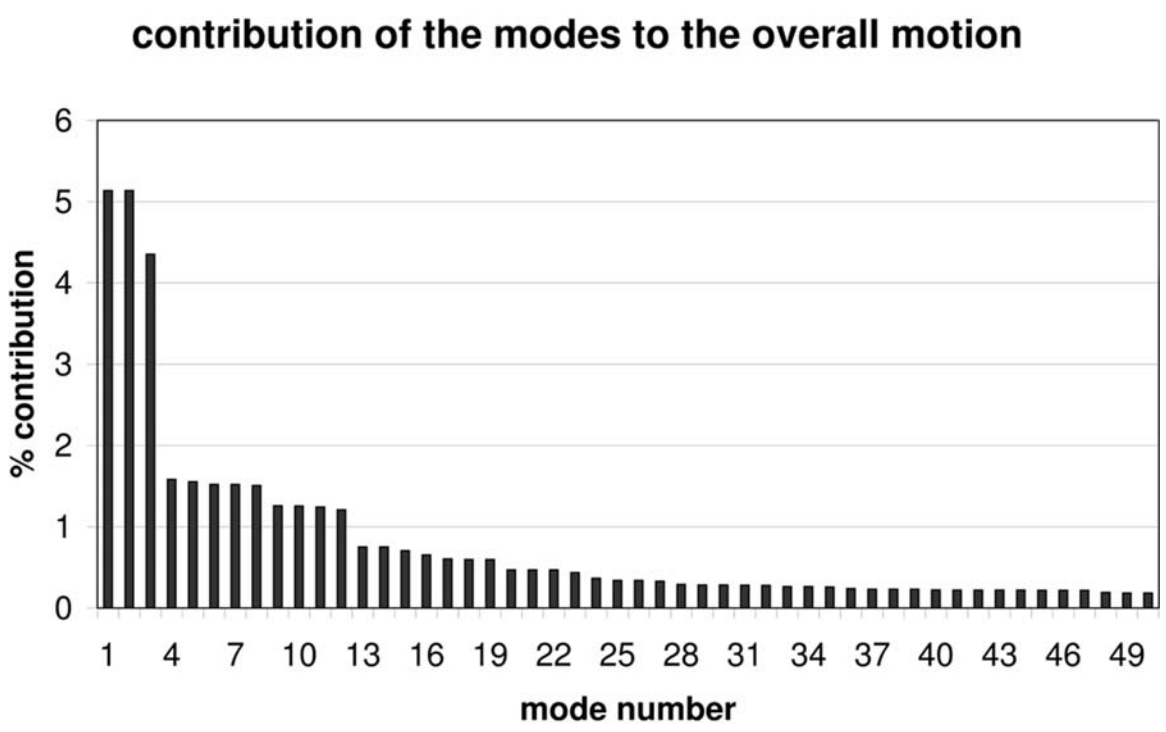
contribution of the modes to the overall motion
% contribution
0
1
2
3
4
5
6
1
4
7
10
13
16
19
22
25
28
31
34
37
40
43
46
49
mode number

Figure S2

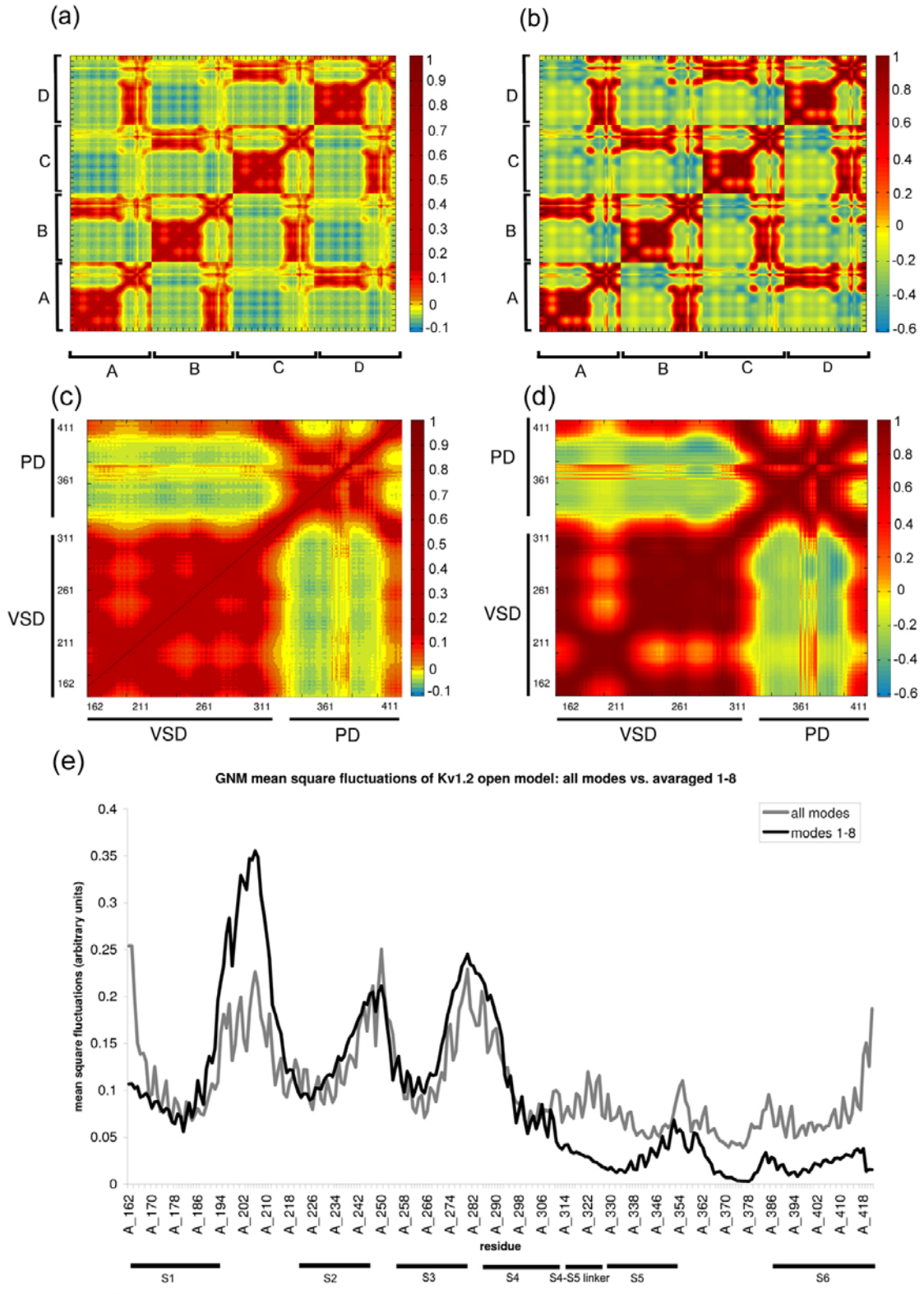
(a)
(b)
(c)
(d)
(e)
D
C
B
A
PD
VSD
GNM mean square fluctuations of Kv1.2 open model: all modes vs. avaraged 1-8
all modes
modes 1-8
mean square fluctuations (arbitrary units)
residue
S1
S2
S3
S4
S4-S5 linker
S5
S6

Figure S3

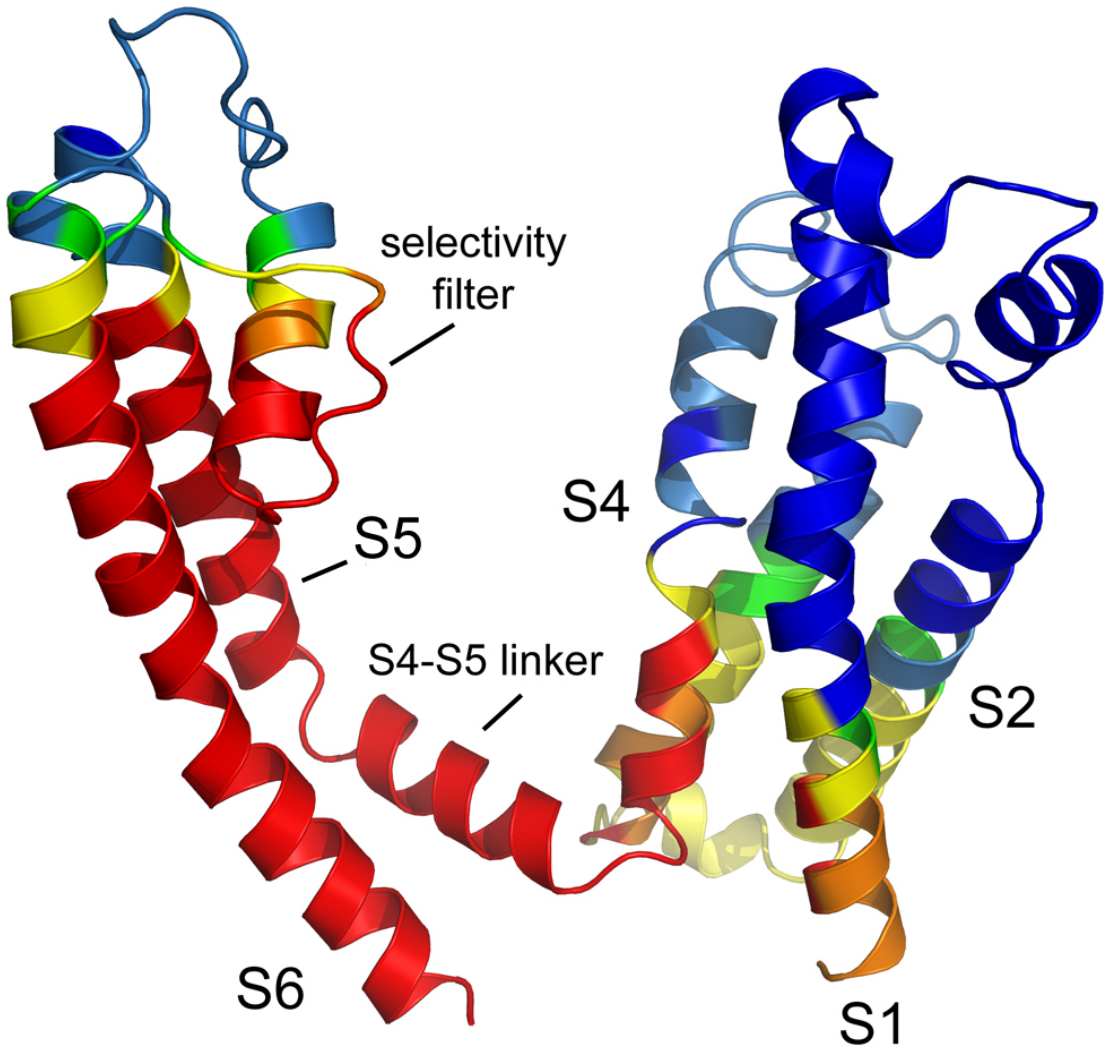

Figure S4

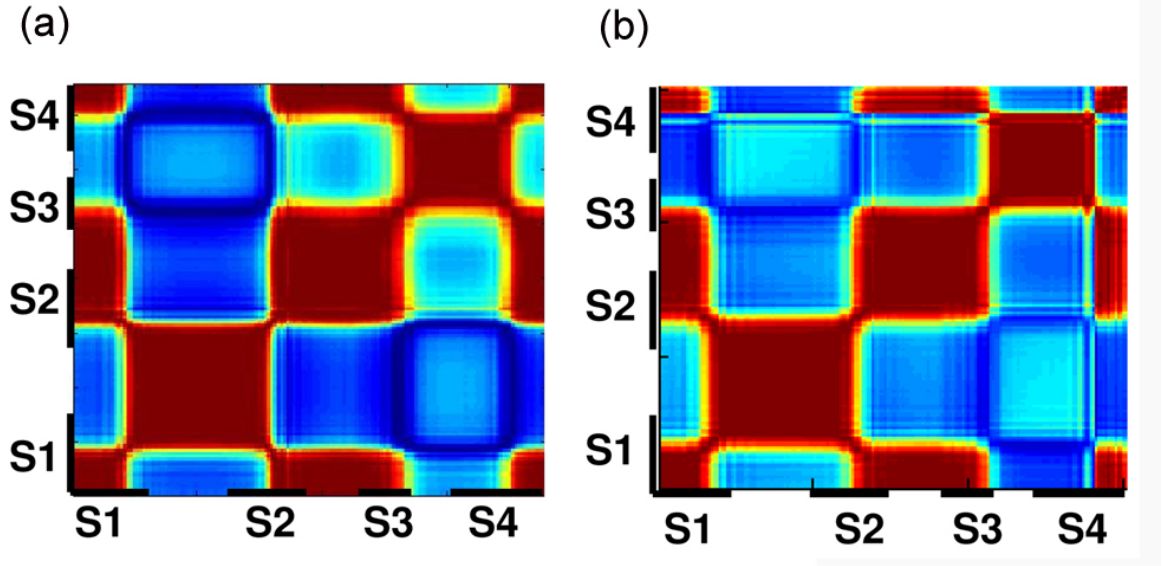

Figure S5

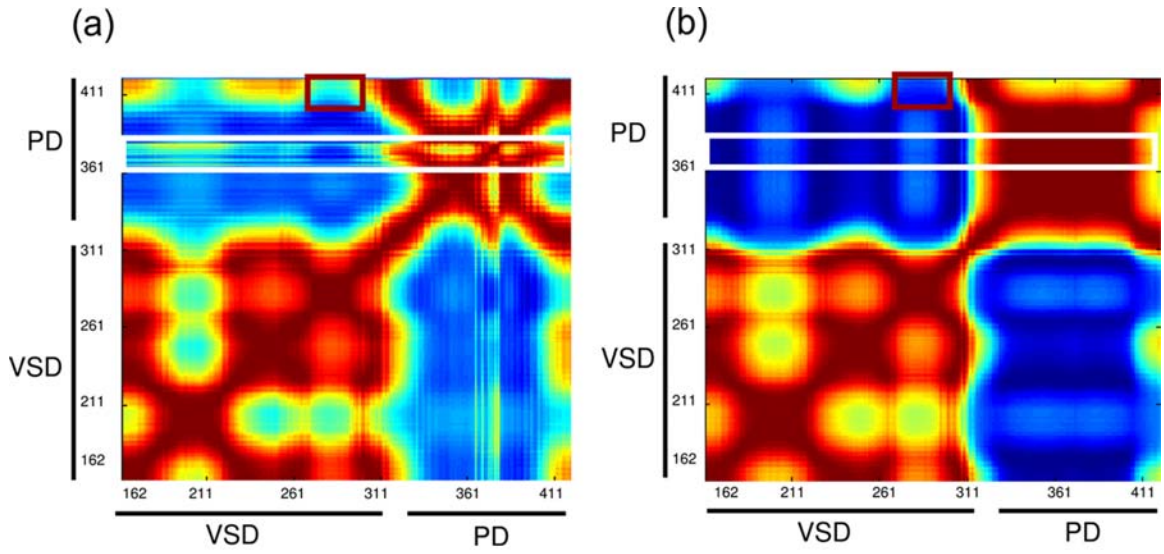

Figure S6

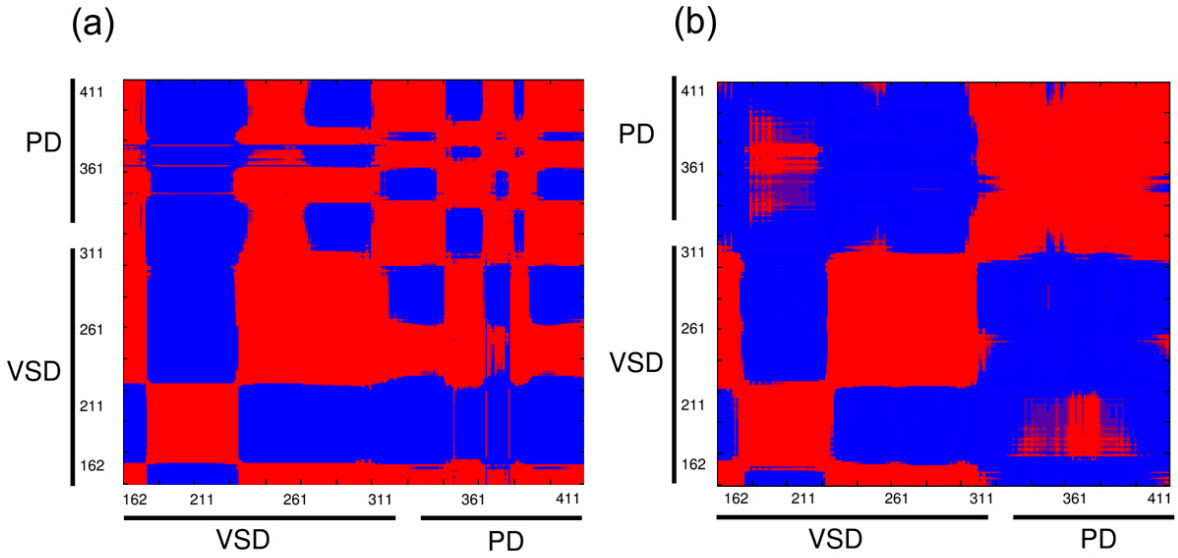

Figure S7

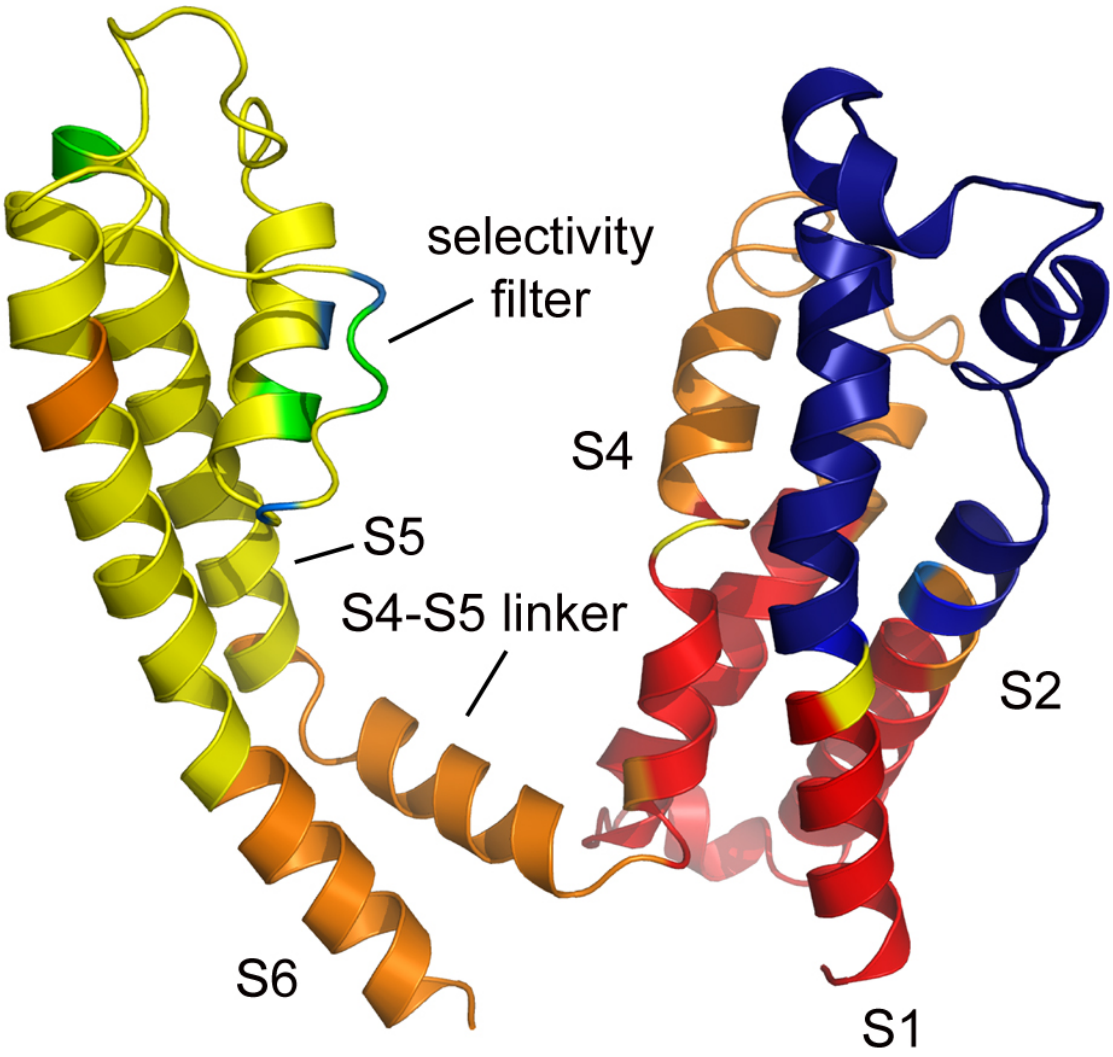

Figure S8

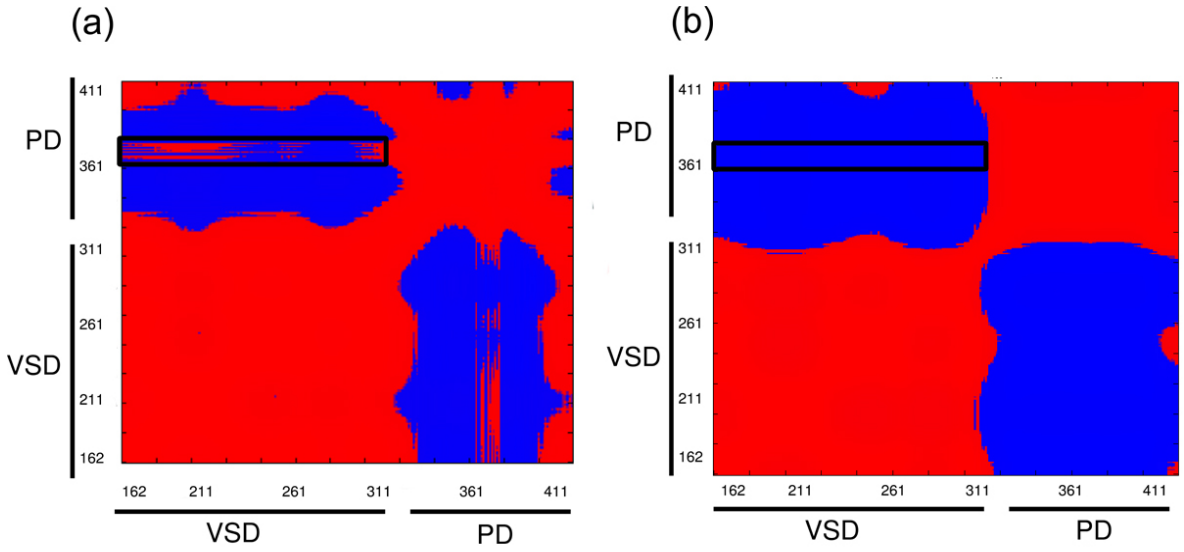

Figure S9

(a)

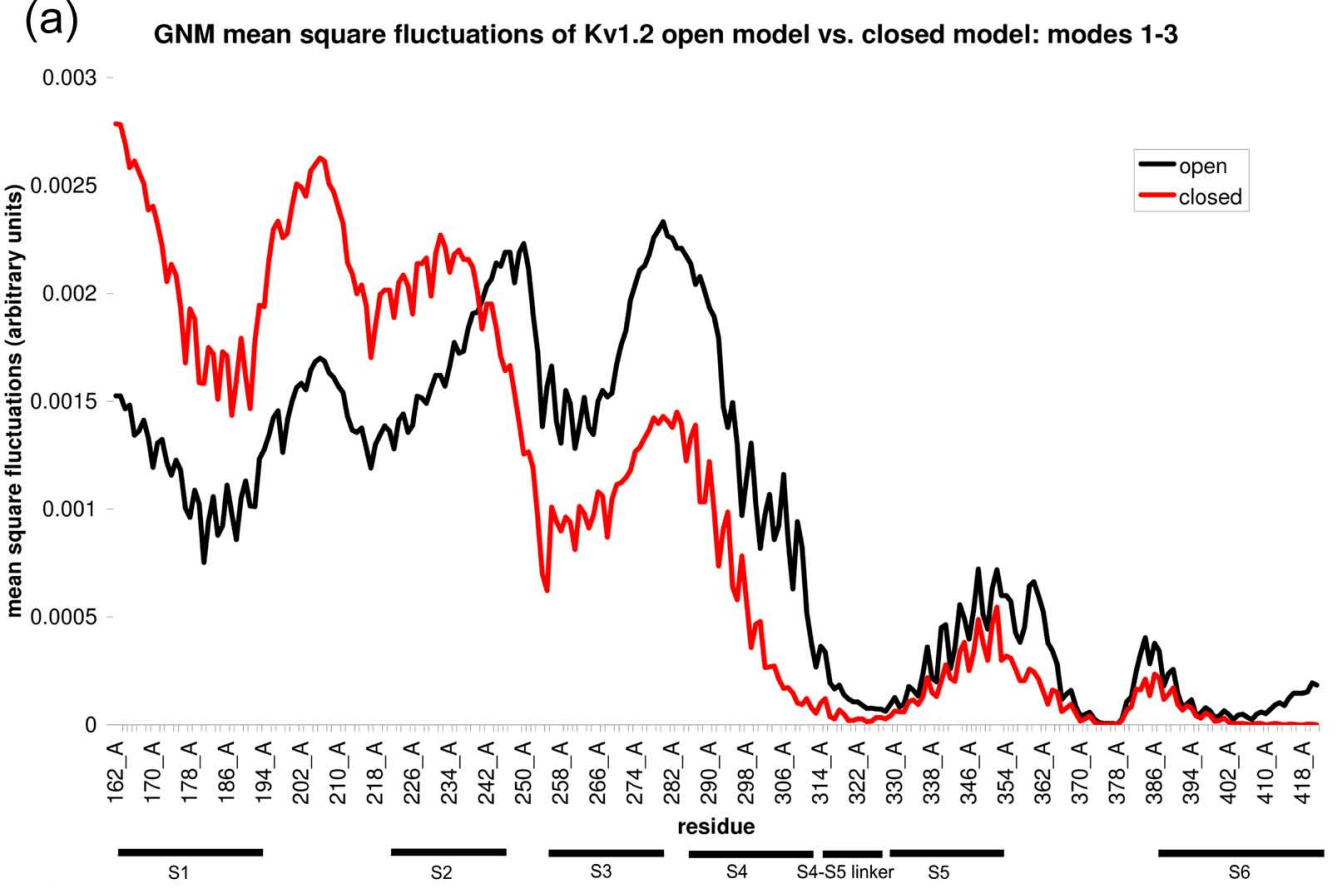

(b)

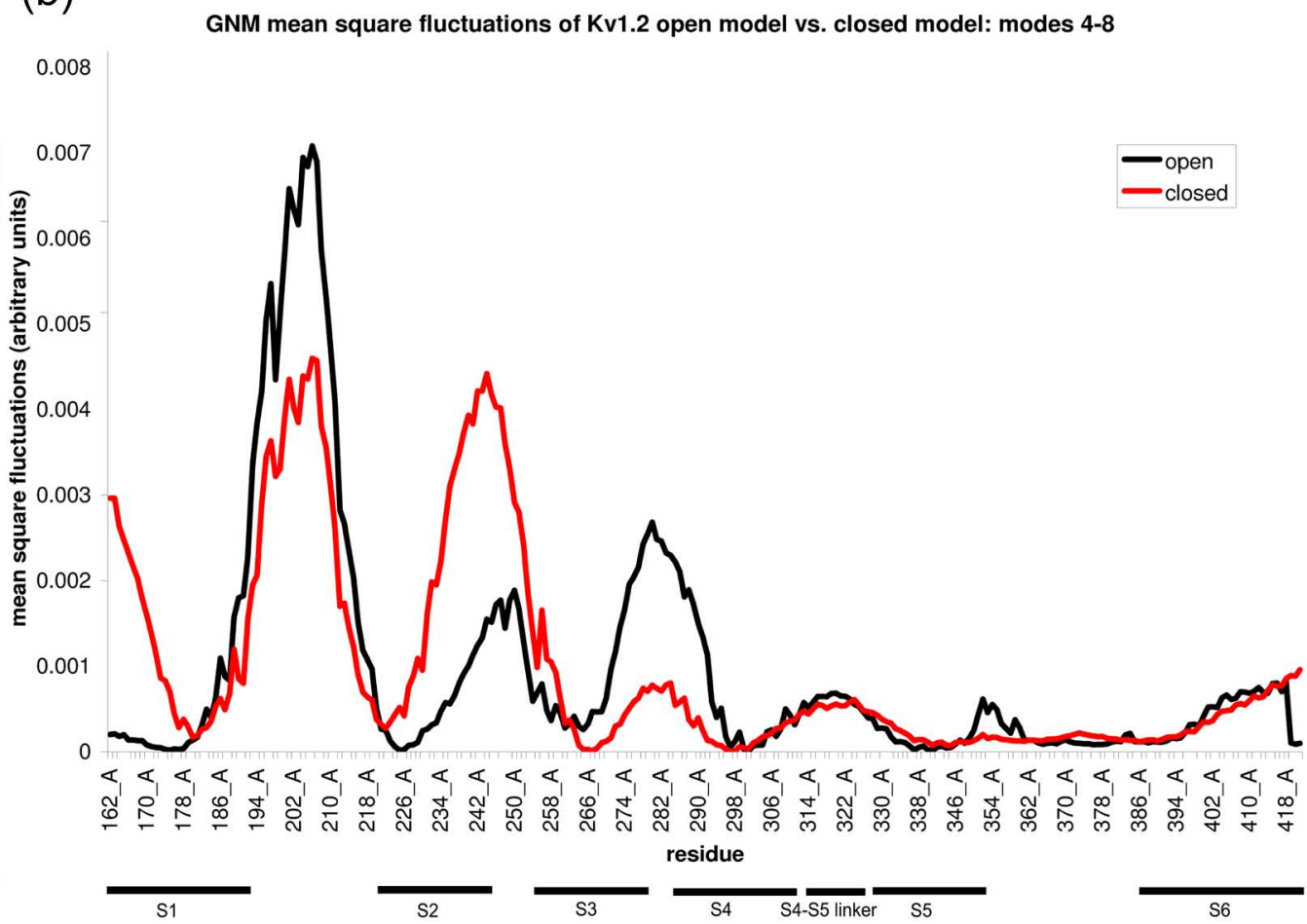

Figure S10